Characterization of $Cs(Pb/Ti)X_3$ Perovskites

Abishrant Panday and Joyce Tian

I. Introduction

The perovskite structure, so named after calcium titanium oxide ($CaTiO_3$), takes a general ABX_3 form with X an anion that binds to cations A, B of significantly differing sizes. Beyond their mineral properties, however, the general perovskite structure, in the organic-inorganic halide form, has seen widespread photovoltaic research within the past decade [1]. In these applications, B is traditionally Pb^{2+} and A is Cs^+, $CH_3NH_3^+$, or $NH_2CHNH_2^+$, with X being a halide anion [2]. Within these configurations, iodide and bromide have shown the most promise in theoretical and practical solar cell properties [3].

The solar cell industry, which is one of the most active areas in terms of research investment, has traditionally focused on crystalline silicon due to its initially high power conversion efficiency (PCE) and ease of manufacturing [4]. However, in recent years, both the impact of non-renewable silicon resources and their high fabrication costs has motivated research towards alternate candidates. The most promising of these include bulk heterojunction, dye-sensitized, and organic polymer thin-film solar cells, which, while improving availability and reliability, have suffered from poor power conversion efficiency and real-world durability [5,6]. Perovskite solar cells, on the other hand, have been at the forefront of increasing PCE in single-junction and silicon-based tandem cells, with power conversion efficiencies rising from 4% to over 29% in lab conditions within the past decade alone [7,8,9].

The study of perovskite cells, however, is interesting for more than just recent PCE advancements: these materials have a host of interesting properties, with clear strengths and areas for improvement. Specifically, organic-inorganic lead halide perovskites have exhibited desirable optical and electronic features, including a semiconductor-metal transition with high dimensionality, high absorption coefficient, and high conductivity [1,10]. Moreover, they also have highly tunable bandgaps in the range of 1.4 - 1.5 eV, exciton binding energies lower than 50 meV, and are easy to crystallize at low temperature, which aids in the fabrication process [11]. However, these lead halide perovskites also possess undesirable properties, including their negative environmental impact due to potential lead contamination and their common

tetragonal-cubic phase transitions, which tend to occur below solar cell operating temperatures and can affect the band structure and bandgap.

Recent computational and experimental research into perovskite solar cells has focused on their ionic charge transport properties, which are mediated by defect species, and can lead to chemical instability, including current-voltage hysteresis [12,13]. In addition, the effect of ionic conduction and excitonic versus electron charge transport and diffusion has been an important debate that directly affects efficiency and thus manufacturability [14]. With these considerations, this project aims to study the stability and bandgap properties of $CsPbX_3$ perovskites, with an initial aim of characterizing these features for differing halide choices. Then, Sn's potential as a more environmentally friendly replacement for lead in the design is considered, with emphasis on its transition and bandgap.

II. Methods

All electronic structures and material properties were carried out by the Density Functional Theory method using the Quantum Espresso package [15].

First, the crystal structures of $CsPbBr_3$, $CsPbI_3$, $CsTiBr_3$, and $CsTiI_3$ were created. Then, the k-point grid size and plane-wave cutoff energy were optimized for the first structure and then utilized throughout the calculations. In our case, a k-point grid size of $8 \times 8 \times 8$ was used, along with an energy cutoff of 40 Ry (544 eV) since it converged within 5 meV/atom of the $16 \times 16 \times 16$ and 100 Ry cases, respectively. With these determinations, the equilibrium lattice constant for each structure was determined and then compared with literature.

After this, the existence of a phase transition for the perovskites was studied by examining the displacement of Pb/Sn atoms in each unit cell and computing energy as a function of displacement for each setup. In addition, we adjusted cell volume by fixing the lattice parameter, allowed the system to relax fully, and calculated system pressure order to determine the existence of a pressure-driven phase transition.

Then, the band structure of each crystal was computed by first running a 'vc-relax' calculation and then a 'bands' calculation. The k-axis is taken as a path along the $\Gamma - X - M - R \; - \; \Gamma - R - X - R$ of the cubic lattice. From this, the band gap energy and the photon wavelength were determined for all crystals. After the bandgap had been determined, the

same calculation was run at multiple cell volumes (and consequently different pressures) in order to determine whether a phase transition could be determined as a band-gap discontinuity as a function of pressure.

III. Results

A. Simulation Parameters and Equilibrium Lattice Constant

As noted above, energy was first computed as a function of k-point grid size and of plane-wave cutoff energy for $CsPbI_3$, yielding a k-point grid size of $8 \times 8 \times 8$ and an energy cutoff of 544 eV (40 Ry) as the values within convergence. Then, for each structure, energy was plotted as a function of lattice parameter and a quadratic curve of best fit was determined, whose minimum allowed for the determination of equilibrium lattice parameters, which are within a reasonable margin of literature [16]:

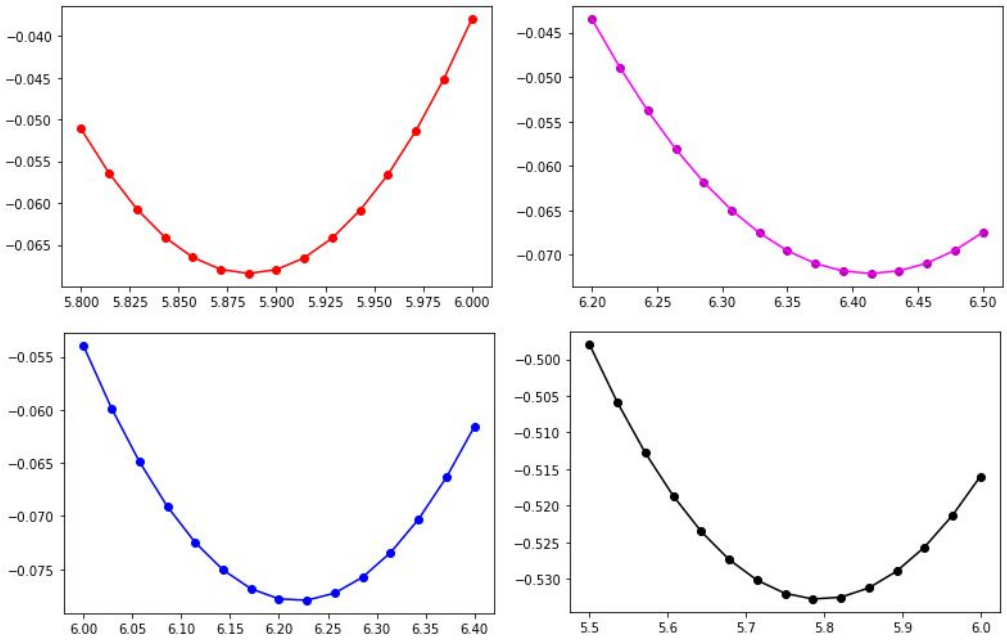

Figure 1: A plot of total energy in eV versus lattice parameter in angstroms for $CsPbBr_3$ (red), $CsPbI_3$ (magenta), $CsSnI_3$ (blue), and $CsSnBr_3$ (black).

Molecule	Lattice Constant (Å)	Literature [16]
$CsPbI_3$	6.394	6.428
$CsPbBr_3$	5.876	5.874
$CsSnI_3$	6.217	6.219
$CsSnBr_3$	5.792	5.795

Table 1: Lattice constant as determined by the minimum of best fit curve for each perovskite.

B. Perovskite Phase Transition

Many perovskite structures exhibit a tetragonal-cubic phase transition, which was initially explored by examining the impact of Pb and Sn displacement on total energy for $CsPbBr_3$ and $CsSnBr_3$, respectively. It was found that both structures exhibited a slight energy discontinuity with respect to stretching of their respective ion.

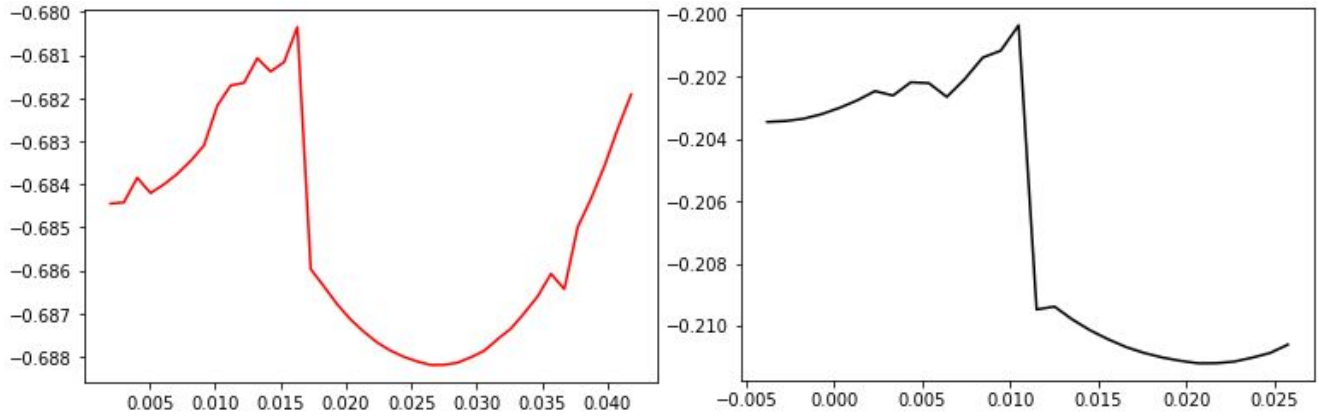

Figure 2: A plot of total energy (eV) versus displacement (scaled by lattice constant in Å) for $CsPbBr_3$ (red) and $CsSnBr_3$ (black).

The existence of this transition was further explored by examining unit-cell volume as a function of pressure, where both structures showed a characteristic discontinuity at 1.15 GPa for $CsPbBr_3$ and at 0.95 GPa for $CsSnBr_3$.

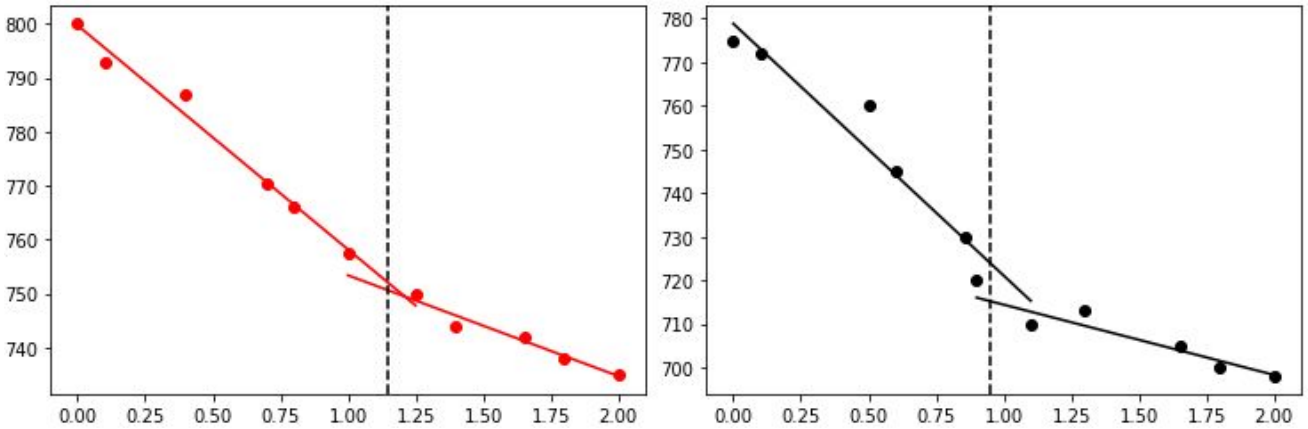

Figure 3: A plot of cell volume (in cubic angstroms) vs pressure (GPa) for $CsPbBr_3$ (red) and $CsSnBr_3$ (black). Dashed lines show estimated discontinuity based on r^2 loss.

C. Band Structure and Bandgap

For both $CsPbBr_3$ and $CsSnBr_3$ the band structure was determined and the valence band maximum (VBM) and conduction band minimum (CBM) for each were plotted on the same

graph. The bandgap was then determined to be the difference between the highest value in the valence band and lowest value in the conduction band.

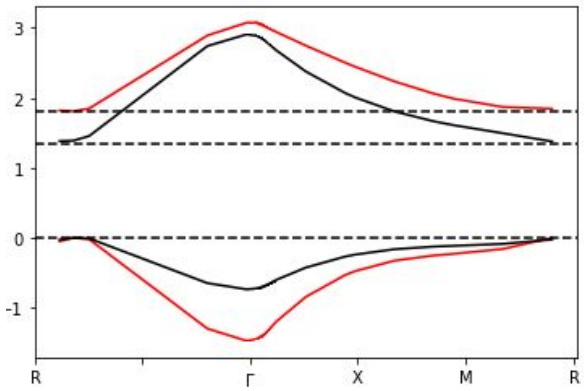

Figure 4: A plot of energy (eV) vs k-point showing the highest valence band and lowest conduction band for $CsPbBr_3$ (red) and $CsSnBr_3$ (black). Dashed lines show minima (0 eV) and maxima (1.34, 1.8 eV).

From this, we get that the bandgap energy for $CsPbBr_3$ is 1.8 eV and for $CsSnBr_3$ is 1.34 eV, both of which are lower than experimental values of 2.012 eV and 1.98 eV since DFT commonly underestimates these [17,18]. In addition, we can calculate the minimum wavelength required to promote an electron from the valence to conduction band as $\lambda = \frac{hc}{E}$, where E is the bandgap. This calculation tells us that $\lambda = 690\ nm$ for $CsPbBr_3$ and $\lambda = 926\ nm$ for $CsSnBr_3$.

Finally, we studied the bandgap evolution of both structures as a function of pressure, which showed discontinuity and confirmed our earlier finding on structural transition. With this study, we saw that $CsPbBr_3$ exhibited a phase transition at around 1.2 GPa and $CsSnBr_3$ at around 0.98 GPa.

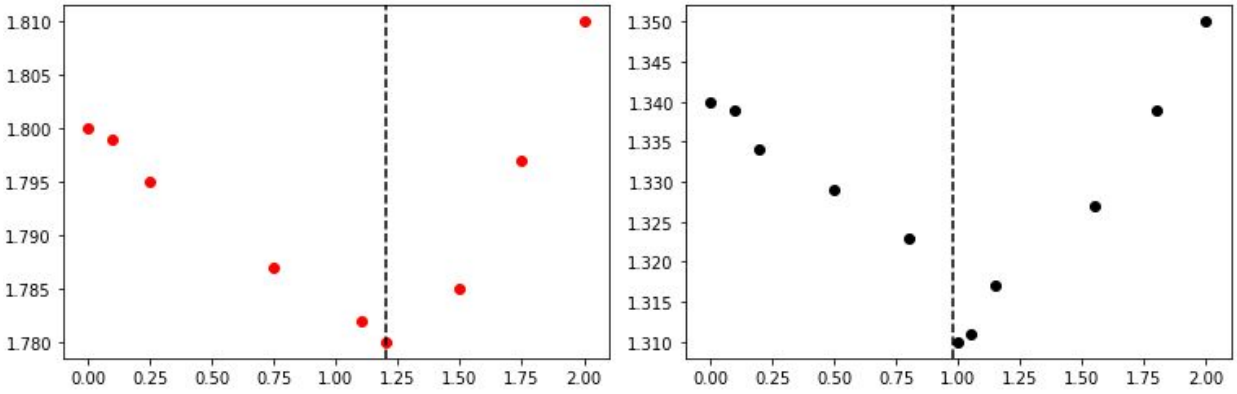

Figure 5: A plot of bandgap (eV) vs pressure (GPa) for $CsPbBr_3$ (red) and $CsSnBr_3$ (black). Dashed lines show phase transition estimates.

IV. Discussion

In our project, we first determined the lattice parameter for each crystal and saw that our results were within a reasonable margin from experimental studies and other theoretical predictions [16]. Then, we studied the phase-transition behavior of perovskites, which is one of the structure's biggest detriments since it occurs at operating conditions for solar cells. We posited Sn as a more environmentally friendly alternative to Pb but found that both exhibited the aforementioned transition regardless. Then, we computed the bandgap structures of $CsPbBr_3$ and $CsSnBr_3$, using that to determine their bandgaps and thus the minimum wavelength required to push an electron through it. Here, we saw that the value determined for both structures was significantly different from experimental values in literature due to the nature of DFT. Finally, we used band gap calculations as a function of pressure to reaffirm our transition pressure determined before.

Because one of our members was ill for a significant portion of the project, there are still some interesting avenues of research that we didn't get the chance to finish exploring: in particular, the effect of ionic contaminants, such as Li^+, into the perovskite layer is a common reason for solar cell failure and studying the effects may yield interesting insights. Moreover, the main mode of energy transport when perovskite is used as an active layer is exciton transport, so the study of exciton diffusion lengths as a function of halide or cation is an option. Finally, due to computational limits, only Cs was used as our central cation. In order to make the results more applicable to the current state of the art, a $CH_3NH_3^+$ center should be used. Our attempts to model the methylammonium center unfortunately resulted in energy calculations which didn't seem to converge at all meaningfully for sizes up to $16 \times 16 \times 16$, indicating such calculations should be run at very large cell sizes, which meant computationally expensive calculations such as relaxation or band gap structure were not completed within our project timeframe.

V. References

[1] Luo, S., & Daoud, W. A. (2015). Recent progress in organic–inorganic halide perovskite solar cells: mechanisms and material design. *Journal of Materials Chemistry A*, 3(17), 8992-9010.

[2] Berry, J., Buonassisi, T., Egger, D. A., Hodes, G., Kronik, L., Loo, Y. L., ... & Mitzi, D. B. (2015). Hybrid organic–inorganic perovskites (HOIPs): Opportunities and challenges. *Advanced Materials*, 27(35), 5102-5112.

[3] Gao, P., Grätzel, M., & Nazeeruddin, M. K. (2014). Organohalide lead perovskites for photovoltaic applications. *Energy & Environmental Science*, 7(8), 2448-2463.

[4] Darvishzadeh, P., Babanezhad, M., Ahmadi, R., & Gorji, N. E. (2017). Modeling the degradation/recovery of open-circuit voltage in perovskite and thin film solar cells. *Materials & Design*, 114, 339-344.

[5] Jung, H. S., & Park, N. G. (2015). Perovskite solar cells: from materials to devices. *small*, 11(1), 10-25.

[6] Jeon, N. J., Noh, J. H., Kim, Y. C., Yang, W. S., Ryu, S., & Seok, S. I. (2014). Solvent engineering for high-performance inorganic–organic hybrid perovskite solar cells. *Nature materials*, 13(9), 897-903.

[7] Park, N. G. (2013). Organometal perovskite light absorbers toward a 20% efficiency low-cost solid-state mesoscopic solar cell. *The Journal of Physical Chemistry Letters*, 4(15), 2423-2429.

[8] Snaith, H. J. (2013). Perovskites: the emergence of a new era for low-cost, high-efficiency solar cells. *The journal of physical chemistry letters*, 4(21), 3623-3630.

[9] NREL Cell Efficiencies, 2020. https://www.nrel.gov/pv/assets/pdfs/best-research-cell-efficiencies.20190802.pdf

[10] Park, N. G. (2015). Perovskite solar cells: an emerging photovoltaic technology. *Materials today*, 18(2), 65-72.

[11] Targhi, F. F., Jalili, Y. S., & Kanjouri, F. (2018). MAPbI3 and FAPbI3 perovskites as solar cells: Case study on structural, electrical and optical properties. *Results in Physics*, 10, 616-627.

[12] Eames, C., Frost, J. M., Barnes, P. R., O'regan, B. C., Walsh, A., & Islam, M. S. (2015). Ionic transport in hybrid lead iodide perovskite solar cells. *Nature communications*, 6(1), 1-8

[13] Yang, D., Ming, W., Shi, H., Zhang, L., & Du, M. H. (2016). Fast diffusion of native defects and impurities in perovskite solar cell material CH3NH3PbI3. *Chemistry of Materials*, 28(12), 4349-4357.

[14] D'innocenzo, V., Grancini, G., Alcocer, M. J., Kandada, A. R. S., Stranks, S. D., Lee, M. M., ... & Petrozza, A. (2014). Excitons versus free charges in organo-lead tri-halide perovskites. *Nature communications*, 5(1), 1-6.

[15] Giannozzi, P., Baroni, S., Bonini, N., Calandra, M., Car, R., Cavazzoni, C., ... & Dal Corso, A. (2009). QUANTUM ESPRESSO: a modular and open-source software project for quantum simulations of materials. *Journal of physics: Condensed matter*, 21(39), 395502.

[16] Jiang, L. Q., Guo, J. K., Liu, H. B., Zhu, M., Zhou, X., Wu, P., & Li, C. H. (2006). Prediction of lattice constant in cubic perovskites. *Journal of Physics and Chemistry of Solids*, 67(7), 1531-1536.

[17] Palazon, F., El Ajjouri, Y., Sebastia-Luna, P., Lauciello, S., Manna, L., & Bolink, H. J. (2019). Mechanochemical synthesis of inorganic halide perovskites: evolution of phase-purity, morphology, and photoluminescence. *Journal of Materials Chemistry C,* 7(37), 11406-11410.

[18] Huang, L. Y., & Lambrecht, W. R. (2013). Electronic band structure, phonons, and exciton binding energies of halide perovskites CsSnCl 3, CsSnBr 3, and CsSnI 3. *Physical Review B*, 88(16), 165203.